Dear Editor,

Thank you for considering our manuscript egusphere-2024-141 ("Multitemporal UAV LiDAR detects seasonal heave and subsidence on palsas") for publication in The Cryosphere. We have been through all feedback provided by you and the reviewers, and we are glad to report that all comments led to changes in the manuscript one way or the other.

In the below, we provide a point-to-point reply to each comment/question raised in RC1, and we specify the changes that were implemented in the manuscript for each of them.

Q = Question / comment raised
A = Answer / details of the changes made

LXXX–XXX refers to the line numbers of text in the revised manuscript.

General comment:

Q1.0: The only major issue I want to raise concerns the error assessment in the study. Surely, the authors present data sets of high quality, but at the same time the vertical differences observed are small. In Tab. 1, the authors state that the vertical accuracy of the digital terrain models presented are 0.021 and 0.028 m for the two different scanners used. In L330-332 it is stated that "changes less than these are within the margin of error", i.e. are not to be interpreted as a reliable signal but rather to be considered as noise. This should be addressed in the study and included in the presentation of the results. When subtracting digital elevation models and creating difference maps, the individual errors should be propagated to separate reliable change information from insignificant change values. Also, it should be clearly stated, how the vertical accuracy presented in Tab. 1 was determined. In assessing the accuracy of the difference models, the "normalization" of the elevation values to the mean mire elevation should also be included and discussed (see specific comments).

A1.0: The main concern the reviewer raises is the error assessment. We do agree with the reviewer that this is required to significantly improve the manuscripts quality. First of all, we have added a more elaborate explanation of how the vertical accuracy by the manufacturer was determined. Our flights were all within the height and velocity ranges for which the scanners are calibrated.

L153–157: The vertical accuracy and precision of these specific LiDAR scanners are determined by the manufacturer. They performed 15 flight lines for YSM+ and 13 for YSM at velocities between 5 and 10 m/s and between heights between 50 and 120 m.a.g.l. over a series of surfaces. The assessment with 18 ground truth points then resulted in the values given in Table 1. All surveys in this study are performed within one year of the calibration.

Next, in the presentation of the results, we have now provided the error range of the height changes. As the reviewer highlights, when subtracting digital terrain (or elevation) models, the individual errors should be propagated. In order to do this, we used the topographic error propagation law (Taylor, 1997):

$$\text{Error of the difference DEM} = \pm \text{Sqrt}(\text{error}_{DEM1}^2 + \text{error}_{DEM2}^2)$$

If we then insert the standard errors from the calibration of the scanners (0.028 for YSM and 0.021 for YSM+), we find the following errors:

September 2022 – April 2023: 0.035
April 2023 – June 2023: 0.030
June 2023 – July 2023: 0.030
July 2023 –September 2023: 0.030

These are now portrayed on Fig. 5 and Fig. 6 (see A1.5), and we added the following to Chapter 3.2:

L211–213: For the change detection, the error range was calculated following the topographic error propagation law (Taylor, 1997), where the propagated error was described as the root sum of squares (RSS) of individual errors. For the individual errors, those described in Table 1 were used.

In order to assure the reader that the main findings of our study are greater than these calculated error margins, we have included the following:

L421–423: The main findings of the study, which include the observed 0.15 m mean heave in winter and associated subsidence over summer and the identification of a degradation hotspot, are larger than the described error.

Further, when portraying the relative palsa height (Fig. 8), we now also included the associated error bars (see A20). This shows that on the Dome palsa only the step from July 2023 to September 2023 falls within the error range and for the Ridge palsa the step from April 2023 to June 2023. The main conclusion of the study, with a heave of 15 cm and corresponding subsidence over summer still stands.

In order to clarify the process of normalization of elevation values to height values, we have Included the following in the Methods chapter (see A12 in this response for further explanation):

L218–227: For each DTM, the mean elevation of the palsa's surrounding was computed and subtracted from the DTM, which normalizes the elevation of the palsa into the height above the surroundings. Since the definition of palsas is morphological (Harris et al., 1988), the height above its surroundings is per definition the height of the palsa. For the normalization, we used the previously mentioned orthophotos to create a polygon around each palsa, for which the mean elevation was taken per LiDAR flight. Areas containing open water at any of the time steps, either thermokarst lakes directly around the palsas or other ponds, were not included in these polygons. The transformation from elevation to height, simplifies the comparison between the data from the different flights. Since the mire in April was snow-covered, the mire elevation from the closest date (June) was taken for normalizing the April DTM.

Q1.5: Finally, it would be helpful for the reader to see the full distribution of elevation change values for all time stamps in a histogram view, maybe as a supplementary figure.

A1.5: The suggestion to include the full distribution of palsa elevation changes for all the time steps is one that will help the reader to interpret the palsa change more thoroughly. We therefore performed this computation and included the results in the main text, as part of Fig. 6, since we find that these data add valuable insights. We even went a step further and present histograms for different parts of the palsas; the entire palsa (meaning all pixels within the palsa outline), the snow-free parts (all pixels within the snow-free polygons, see Fig. 6a, b, e, f), and finally the degradation hotspot (the quickly degrading 225m^2 part along the northwest edge of the Dome palsa). This distinction makes it clear to the reader that the elevation increase from September 2022 to April 2023 is two-fold: a peak due to the snowfall and a peak due to the heave. The snowfall-peak is mirrored in the following time step (April 2023 to June 2023), after which both the 'entire palsa' and 'Snow-free parts' distributions are mostly similar. Showing the 'degradation hotspot', puts this area in better context of the entire palsa (as asked in Q14), with enhanced elevation losses in all time steps, even after the winter snowfall.
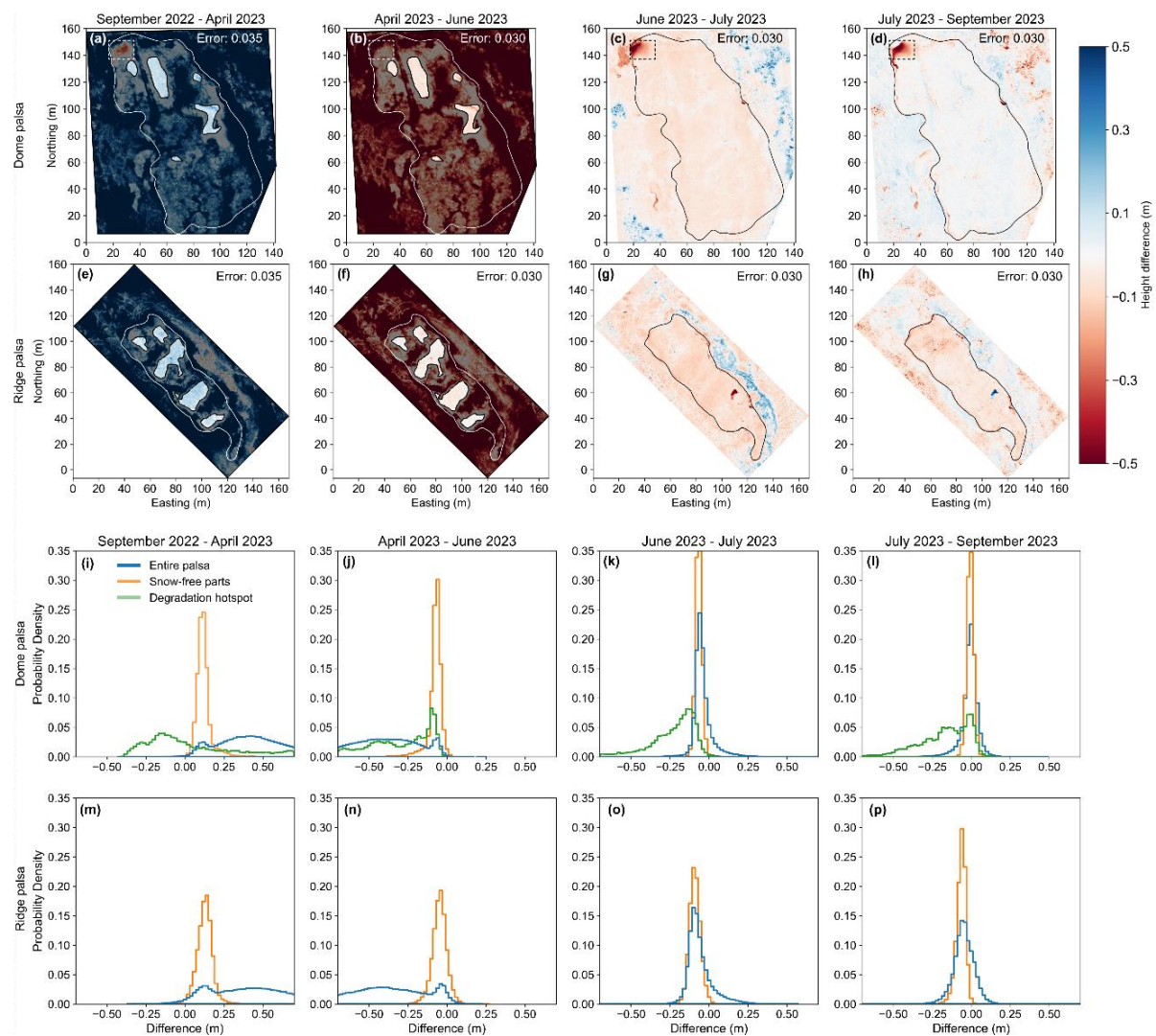
L258–264: **Figure 6 Sequential height difference maps of the Dome (a,b,c,d, with the 'degradation hotspot' in the dashed rectangles) and Ridge (e,f,g,h) palsas between the five UAV LiDAR DTMs from September 2022 to September 2023. Each panel showcases the topographical changes over successive intervals. Blue colors indicate elevation gains and red colors indicate elevation losses. The snow-covered areas (a, b, e, f) are greyed out, leaving the snow-free parts highlighted. Panels i–p display histograms with the distribution of height changes, separated into the entire palsa area (including snow-free parts), snow-free parts only, and the 'degradation hotspot' on the Dome palsa.**

The added histograms are now also addressed in the main text of Chapter 4.2, which is also revised to improve the readability:

L244–255: **4.2 Seasonal terrain changes from UAV LiDAR**
By comparing DTMs from consecutive periods, we observed intra-annual terrain variations, i.e., frost heave and thaw subsidence on the two studied palsas. Change maps for the different time steps are shown in Figs. 6a–h, while Figs. 6i–p are corresponding histograms of change. The first two time steps are largely affected by snow cover in April, hence the histograms of change show both the entire palsa as well as only the snow-free parts (Figs. 6i–p).

On the snow-free crests there was an elevation increase (heave) of up to 0.30 m and on average of 0.15 m from September 2022 to April 2023 for both palsas (Figs. 6a and 6e). Between June and July, both palsas clearly subside over the whole area (Figs. 6c and 6g), on average 0.05 m on the Dome palsa and 0.08 m on the Ridge palsa. Subsidence from July to September is only clear on the Ridge palsa, with 0.05 m on average over the entire palsa (Fig. 6h). Despite being snow-covered in April, the degradation hotspot in the northwestern part of the Dome Palsa displayed a height decrease of up to 0.4 m between September 2022 and April 2023 (Fig. 6a and 6i), indicating that subsidence in this area also occurred between these months.

L265–272:
Figure 7 shows a time series of elevation changes along profiles, providing another way to look at the heave and subsidence. The degradation hotspot is seen in Figs. 7c and 7e, where this area progressively degraded vertically up to 1.9 m between September 2022 and September 2023. The ATV track that crosses the Dome palsa shows a subsidence of 0.2–0.3 m just over the time period in this study (at ca. 27–29 m in Fig. 7e). On the Ridge palsa it can be seen in Figs. 7f and g that the subsidence was greater in the depressions than on the crests., The heterogeneous snow cover is visible in Figs. 7c and d. The snow thickness is up to ca. 2.0 m at the eastern margin of both palsas and 1.0 to 1.5 m in the depressions, while the crests remain snow-free (also see Fig. 1d).

Specific comments:

Q2 L79-81: I recommend to shift this sentence to the conclusions

A2: After revising the Introduction, we agree that this belongs in the Conclusions and have removed this sentence.

Q3: L88-91: In my view, it would be good to also provide the area of the two palsa features here. This would allow the authors to quantify the areal change, as well as to describe the features more comprehensively.

A3: We thank the reviewer for this suggestion, which does help describe the palsas more comprehensively. This comment also made us realize that that the approximated width and length values were in 2023 and not 2022. We have fixed that and have included the area of the two palsas in the text.

L101–104: In September 2023, the Dome palsa was approximately 170 meters in length and 75 meters in width, with an area of 11408 m² and its highest point about 4 meters above the surrounding mire. The Ridge palsa measures about 125 meters in length and 40 meters in width, with an area of 3522 m² and its highest point being roughly 5 meters above the adjacent mire terrain.

Q4: L92: all-terrain vehicle (ATV)

A4: We have now included the definition of ATV.

L105–106 An all-terrain vehicle (ATV) track runs over the northeastern part of the palsa,

Q5: L98: Please provide coordinates detailing the locations of panels b) and c) as well. Also, b) would deserve a scale bar. The resolution of the Figure could also be improved, though this is likely related to the preprint format and will be accounted for in the full publication.

A5: We agree with the reviewer that all maps should have coordinates to highlight their location. The same goes for a scalebar. We have adjusted the figure accordingly and also took the opportunity to make all scalebars of the same style. Regarding the resolution of the figures, we can assure that each figure is exported at high resolution and will be high quality for the publication.
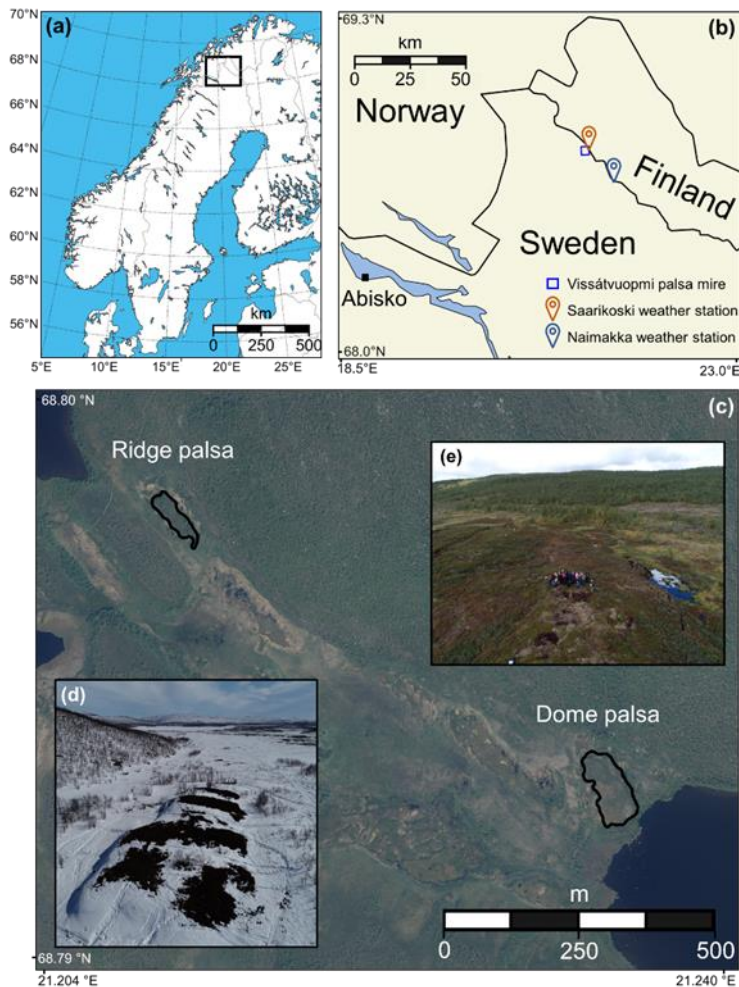
Q6: L115-116 / L122-123: If the HOBO station has been installed in September 2022, how can the data shown in the lower panel (add letters) of Figure 2 show monthly precipitation and snow depth before that date?

A6: For the dates before September 2022, we used the Naimakka station (see Fig. 1), which is operated by the Swedish Meteorological Institute (SMHI) since 1944. In order to clarify this, we have included the establishment data of the Naimakka weather station in the text.

L127–129 The Köppen climate type is Subarctic (Dfc) and a weather station operated by the Swedish Meteorological Institute (SMHI) in Naimakka (established in 1944), ca. 18 km east of the study site observed a mean annual air temperature of of -1.5 °C and mean annual precipitation was 460 mm in the 1991–2020 standard period.

Finaly, we have added letters to the two panels of Fig. 2.

Q7: L121-122: Does "Air temperature" refer to mean daily air temperature? Please specify this here and also elaborate in the text at which interval the temperature is recorded.

A7: The 'Air temperature' refers to mean daily air temperature. This is recorded every two hours. We have included clarification in the text:

L137–138: Mean daily air temperature at ca. 1.5 km (Saarikoski) and at ca. 18 km (Naimakka) from the studied palsas.

L132–133 At this station, air temperatures at 2 m above the ground surface are recorded at two-hour intervals.

Q8: L124-125: These are interesting details from an earlier study. I would encourage the authors to come back to this data in the discussion and compare their 2022-2023 area changes to those found by Olvmo et al. before. Again, this would involve delineating the exact position of the palsas in the data presented here, which in my view would increase the quality of the work. It would also help to show the outlines of the palsa features in Figures 5 to 7.

A8: The reviewer suggests including outlines of the palsas extent in figures 5–7, which we agree would greatly improve these figures and the ease of interpretation. We used orthophotos, created with a DJI Phantom 4 on the same days as the LiDAR surveys, in order to draw the outlines of both palsas in 2022 and 2023. For the Dome palsa, the southern margin is relatively unclear in the DTMs as the landform flattens out here. In the orthophotos however, a clearer shift in wet-dry vegetation can be followed along this margin.

L239–240: The black lines represent the extent of the palsas, based on orthomosaics from the same day as the UAV LiDAR surveys.

The suggestion to compare areal losses from our study to Olvmo et al. (2020) helps to put our study in the context of the region. However, since one-year area losses are not representative for a robust signal, we decided to compare the palsa area changes from Olvmo et al. (2020) with the 2016–2023 area loss. For this, we used the aera of both palsas in 2016 (from Olvmo et al. (2020)) and the 2023 areas from our study. We then calculated the % area loss per year for 2016–2023. The values and discussion of these is now included in the Discussion chapter.

L387–398: Olvmo et al. (2020) found an average annual decay rate (loss of palsa area) of -0.74 %a−1 and -2.45 %a−1 for the Dome and Ridge palsas respectively, for the period 2010–2016. Using the palsa area from Olvmo et al. (2020) in 2016 and the extent in 2023 from our study, we can calculate a new annual decay rate. For the period 2016–2023, we found respective rates of -3.27 %a−1 and -1.55 %a−1. The -2.53 %a−1 change in decay rate on the Dome palsa can be largely explained by the degradation hotspot, which covered ca. 2.6% of the total palsa area. The slight decrease in annual decay rate on the Ridge palsa could be explained by a stabilization of degraded areas. When excluding the degradation hotspot on the Dome palsa, the Ridge palsa lost a larger percentage of its extent, similar to Olvmo et al. (2020). Again, lateral water fluxes greatly affect ground temperatures and permafrost degradation (Martin et al., 2021; Sjöberg et al., 2016; Walvoord & Kurylyk, 2016). Therefore, smaller palsas are relatively more susceptible to lateral erosion through heat and water fluxes, provided by surrounding thermokarst ponds, compared to larger palsas (e.g. Borge et al., 2017).

Q9: L147: flight missions?

A9: We agree that 'flight missions' is the better term and have changed this in the text.

L167: Table 1. LiDAR scanner and flight parameters of the flying flight missions.

Q10: L152: superscript m2

A10: We thank the reviewer for pointing out this mistake and have fixed it.

L171–172: Similarly, flights over the Dome palsa yielded a slightly larger coverage area of 53993 m^2 compared to the Ridge palsa,

Q11 L185-187: Why did the authors decide to use the minimum elevation here? Would the high point density also allow to use the 25th percentile of the distribution to determine the elevation of a cell to not be relying on individual points that also might deviate from the surface?

A11: The reviewer asks why we used the lowest point in each 0.10x0.10 m area when creating a DTM, as opposed to the 25th percentile. The vegetation on these palsas is low and compact, meaning that some vegetation might not be filtered out by the ground classification algorithm. By taking the lowest point, we are confident that we create a terrain model that represents the ground surface. We agree that by taking the lowest points, the chance for using outliers in the data is increased. In order to address this point, we performed a test on the point clouds (from September 2023), where we take 100 random 0.10x0.10 m areas on each palsa and compare the minimum elevation with the 25th percentile of the data. The results are presented below and show a coefficient of determination, R^2, of 1.00 and mean absolute error (MAE) of 0.02 m for both tests. This means that the lowest elevation and the 25th percentile elevation correlate perfectly and that the latter is on average 0.02 m higher than the lowest points. It shows that the random areas contained no outliers.
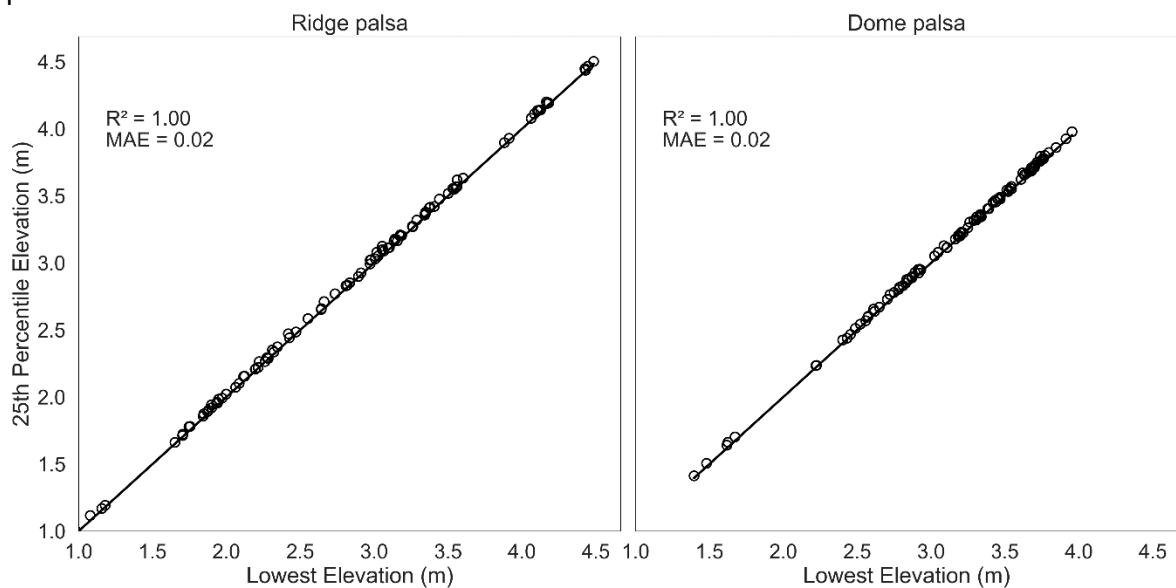
In order to address this point in the main text, we included the following:

L207–209: A comparison of the lowest point and the 25th percentile elevation in 100 random 0.10 by 0.10 m areas on each palsa was carried out, which showed no outliers at the ground level.

Q12: L191-195: But the mire elevation cannot be considered constant, as the authors also describe in L273-277. Given the small overall differences between the DTMs produced for the different time-stamps, how can the authors make sure that these are not produced by the normalization process to a fluctuating mire surface elevation?

A12: An important note to make is that the definition of a palsa is morphological and thus per definition the height above the surroundings is the height of the palsa. That fact that the elevation of the mire cannot be considered constant is therefore the reason to do the normalization. The polygons surrounding the palsas that we used for the normalization are carefully drawn to not include open water bodies.

We have elaborated this further in the Methods chapter:

L218–227: For each DTM, the mean elevation of the palsa's surrounding was computed and subtracted from the DTM, which normalizes the elevation of the palsa into the height above the surroundings. Since the definition of palsas is morphological (Harris et al., 1988), the height above its surroundings is per definition the height of the palsa. For the normalization, we used the previously mentioned orthophotos to create a polygon around each palsa, for which the mean elevation was taken per LiDAR flight. Areas containing open water at any of the time steps, either thermokarst lakes directly around the palsas or other ponds, were not included in these polygons. The transformation from elevation to height, simplifies the comparison between the data from the different flights. Since the mire in April was snow-covered, the mire elevation from the closest date (June) was taken for normalizing the April DTM.

Further, the addition of the histograms in Fig. 6 (see Q1.5) further strengthens this. Since almost the entire distribution of changes to April 2023 (Fig. 6i, m) show an increase in palsa height and accordingly changes from April 2023 to June 2023 a decrease (Fig. 6j, n), which is in line with the hypothesis of frost heave and thaw subsidence on permafrost landforms.

Finally, we have added to the Discussion, where we describe that each correction of elevational data brings uncertainties, especially in a landscape so dynamic as a palsa mire. But we are confident that the presented height changes are related to the dynamics of the palsas.

L320–327: A process other than freeze-thaw dynamics that could have affected the LiDAR measurements is the seasonal oscillation of the peatland surface height due to water table fluctuations, called 'mire breathing' (Kellner & Halldin, 2002; Roulet, 1991). By accounting for the elevational changes in the ground surface of the surrounding mire (and thus not open water), we ensure that the presented height values reflect height of the palsa mounds and thus hold true to the morphological definition of palsas. Since palsa mires are very dynamic landscapes, each correction brings uncertainties. The closely aligned elevation

profiles (Fig. 7) give us confidence that the presented height changes are primarily a result of freeze-thaw dynamics of the palsas.

Q13: L198-199: Please elaborate in more detail how this height difference was calculated and how the vertical accuracy might influence the interpretation. Is the maximum difference provided here based on a single pixel? How confident are the authors that this provides a robust signal?

A13: These values were based on the single 0.10x0.10 m pixel with the highest elevation on the dataset (per palsa) and thus do not represent a robust signal. We thank the reviewer for pointing this out and removed the statement as it takes away from the main message of the Results section. Section 4.1 is now rewritten.

L230–236: Between September 2022 and September 2023, both palsas underwent degradation along their margins (Fig. 5). The largest height change was observed along the northwest edge of the Dome palsa, where an area of 225 m² (2.6% of the total palsa area) subsided up to 1.9 m and on average 0.85 m. This corresponds to a 34% height loss on this part of the palsa. From hereon we name this 225 m² area the 'degradation hotspot'. Degradation also occurred within the ATV track that borders the eastern side of this degradation hotspot. The height of the Ridge palsa decreased slightly over the entire landform, with most loss along the margins in the form of lateral degradation.

Q14: L199-202: It would be interesting to place these 300 m2 in the context of the full extent of the feature. What is the percentage change?

A14: We agree that this area (now called 'degradation hotspot') is of interest and therefore we investigated this in more detail. In the process, we found a prior mistake, as this hotspot is 225m^2 as opposed to 300m^2, which adjusted throughout the manuscript. We calculated the areal percentage of the entire palsa that this hotspot covers (2.6%), as well as what the percentage height change within the hotspot area between September 2022 and September 2023 is (34%). This hotspot is now also highlighted in Fig. 5 and Fig. 6. And finally, as part of A1, where we plot the distribution of height changes in Fig. 6, we have also included histograms that cover the degradation hotspot. This further puts that area in context of the entire Dome palsa.

See A13 for the revised Section 4.1.

Q15: L206: In the figure, c) does not show a DTM, but a difference map. Furthermore, providing outlines of the palsas here would help interpreting the figures, especially for panels c) and f).

A15: Figure 5c and 5f show indeed difference maps and not DMTs. We have adjusted the caption accordingly. Outlines are also included (more info about this in A8).

L238–242: Figure 5. DTMs of the Dome (a,b) and Ridge (d,e) palsas on UAV LiDAR scans in September 2022 and September 2023. The black lines represent the extent of the palsas, based on orthomosaics from the same day as the UAV LiDAR surveys. The difference maps (c,f) show the topographical changes over one year, with the palsa extent from the

September 2022 flights in black The dashed box in (c) shows the 'degradation hotspot' on the Dome palsa.

Q16: L211-212: A lot of full stops here

A16: We have removed the second stop.

L270–272: The snow thickness is up to ca. 2.0 m at the eastern margin of both palsas and 1.0 to 1.5 m in the depressions, while the crests remain snow-free (also see Fig. 1d).

Q17: L220: Also in this figure, it would be nice to show the outlines of the palsas to help the reader interpreting the elevation difference shown here. Furthermore, masking the snow covered area in April 2023 here would in my view be advisable to avoid misinterpretation of the figure.

A17: Outlines are now included in Fig. 5–7 (more info about this in A8). The suggestion to mask out the snow-covered area in panels a, b, e and f of Fig. 6 is one that indeed does help the reader to interpret the figure and not be misled. Hence, the updated figure now has the snow-covered areas slightly greyed out, but still visible. This allows the reader to still observe the degradation hotspot in the northwest part of the Dome palsa, which we now also highlight with the dashed box in figures a-d. Further changes to this figure (the error annotation and the inclusion of the full distribution of changes in panels i–p) and its caption are explained in A1.

Q18: L236: Again, please elaborate how these values were calculated. Is the difference in mean height calculated on the entire distribution of the values, or just using a subset on the palsa surface?

A18: These values are computed by using a subset of only the snow-free areas of the palsa surfaces. In order to make this clearer for the reader, we have included the following:

L280–281: The mean height of both palsas, calculated by taking all pixels within the snow-free areas, increased 0.15 m between September 2022 and April 2023 (Fig. 8).

Q19: L238-242: Did the authors analyse whether the individual differences of the intermediate time steps are comparable to the changes determined from subtracting the start and end models?

A19: The question is whether the sum of the individual differences between intermediate time steps is comparable to the change determined by subtracting the start model (September 2022) from the end model (September 2023).

The values here are calculated by taking the mean height of the palsas relative to the September 2022 mean. This means that each intermediate time step (t) equals:

$$\text{meanheight}_t - \text{meanheight}_{sep22}$$

By summing the changes observed in each intermediate period, we inherently obtain the total change from the start (September 2022) to the end (September 2023).

In order to clarify this is in the main text, we included the following in the caption of Fig. 8.:

Q20: L244-245: In this figure, it would be interesting to see error bars for the values of relative height changes.

A20: As part of the error assessment, we have now included error bars for Fig. 8. The error bars represent the scanner specific RMSE for the respective LiDAR scanners used (2.8 cm for September 2022 and 2.1 cm for the other data points). Since for each data point, the mean palsa height is calculated independently, the standard error (and not the propagated error as in Fig. 6) is shown.
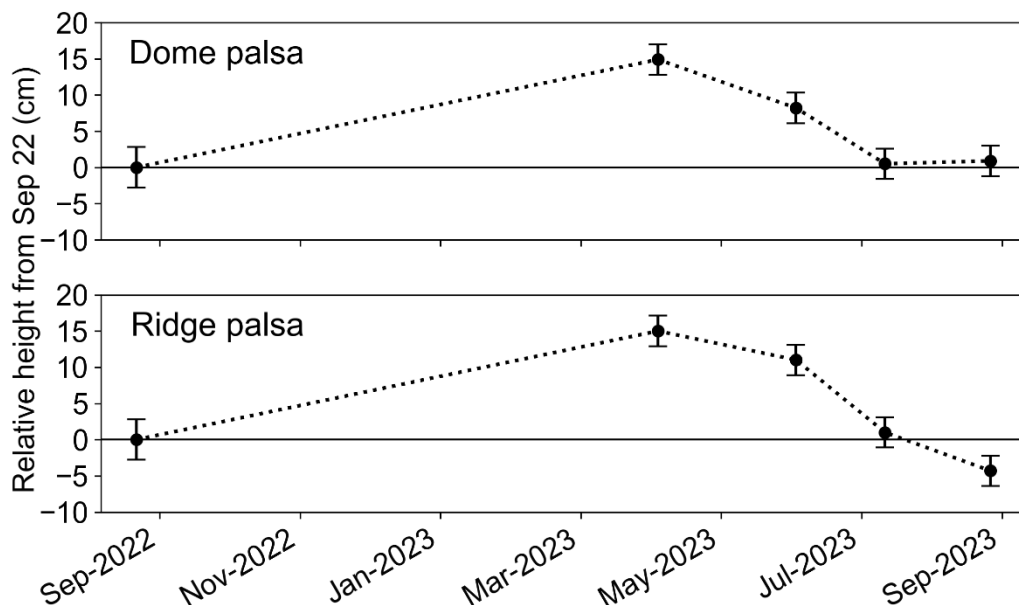
Figure 8. Heave and subsidence on the two studied palsas during the 2022-2023 year. Mean height changes relative to September 2022 are plotted (only for the areas that were completely snow-free in April 2023). The cumulative changes of the intermediate steps add up to the total change from September 2022 to September 2023. The error bars represent the scanner specific RMSE for the respective LiDAR scanners used.

Q21: L268-273: Is there any data that supports the assumption of a thinner active layer in the top-positions of the palsa compared to their surroundings?

A21: We do have active layer data on both of the palsas. We measured the active layer thickness (ALT) by inserting a 1.80 m steel rod until the top of the frozen ground was found. These data are included in Appendix A. Fig. A1 shows the location of the used data points that were filtered for being either within the snow-free crests (TOP) of the palsas (see Fig. 6 for these polygons) or clearly in a lower position or depression (BOT). Fig. A2 then shows the distribution of the ALT at both palsas. The ALT on the top-positions is generally lower and more narrowly spread compared to the points in the lower parts/depressions.

L315–317: The 0.15 m heave is computed on the areas that were snow-free in April and are thus biased towards the crests of the palsas that have a thinner active layer (see Appendix A) as they have a thinner winter snow cover, which limits the insulation of the ground below.

L464–476:
Appendix A: Active layer thickness
The thickness of the active layer (ALT) is measured in September 2023 at both the Dome and the Ridge palsas by inserting a 1.80 m steel rod until the top of the frozen ground was observed. The points (Fig. A1) are either within the polygons of the parts that were snow-free in April 2023 (see Figs. 6a, b, d and e) or in a lower part of the palsa. The former points are assigned 'TOP', while the latter are assigned 'BOT'. The points in the 'TOP' class have a thinner and more narrowly spread ALT compared to the points in the 'BOT' class (Fig. A2).
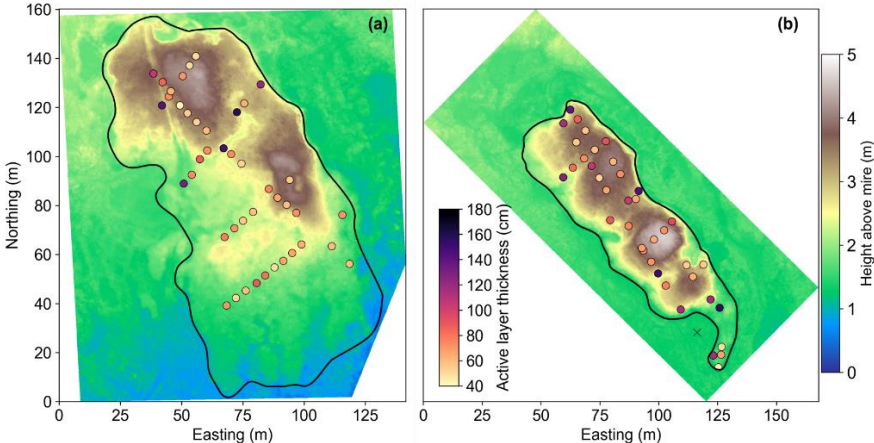
Figure A1. Active layer thickness (ALT) on the Dome palsa (a) and Ridge palsa (b) in September 2023 with their corresponding DTMs.
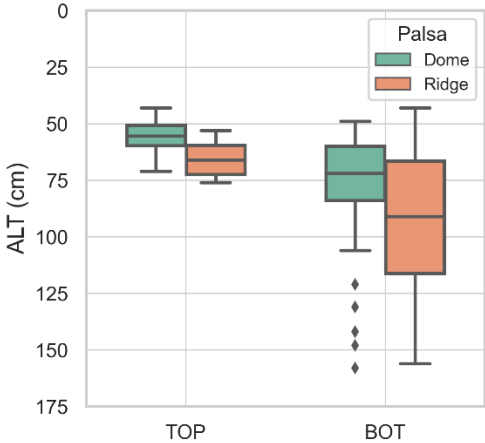
Figure A2. Distribution of the ALT at both palsas, showing that ALT in the top-positions is generally lower and more narrowly spread compared to the points in the lower parts or depressions.

Q22: L308-311: This aspect should be discussed in more detail here. While I agree that the elevation changes on both palsas are very similar (L241-242, Fig. 8), the behaviour over the summer is different. Is this a robust signal and what is the interpretation of the authors?

A22: We agree with the reviewer that more discussion regarding the different amounts of lateral degradation and subsidence is needed. Changes to our manuscript with a discussion of lateral decay rates and comparison to values from Olvmo et al. (2020) is already included in A8 in this response. Further hypotheses for the higher rate of subsidence at the Ridge palsa are related to the water bodies that surround this palsa. From our frequent field visits, we know that these are deeper water bodies around the Ridge palsa compared to the Dome palsa, which could enhance water and thus heat fluxes to the palsa core and result in more subsidence. However, these are hypotheses and can only be confirmed by investigations of the palsa interior, for example through geophysical tests. Finally, annual LiDAR surveys (which the authors intend on doing) are required to confirm whether or not this higher subsidence rate is a robust signal or not.

L352–359: In our study, we show that the elevation change of the Dome palsa as a whole from September 2022 to September 2023 was minor and mostly within the 0.030 m error range, while the Ridge palsa did subside on average 0.07 m within one year. A hypothesis for this is related to the surrounding thermokarst ponds. The Ridge palsa is surrounded by relatively larger and deeper thermokarst ponds, which could enhance vertical subsidence more centrally in the palsas as a result of increased heat transfer to the palsa core. To find out if the higher subsidence on this palsa is a robust signal and what processes are responsible for this, continued annual LiDAR surveys and observations of the palsa's interior via geophysical imaging are needed.

Q23: L319: A lot of commas here

A23: We have removed the second comma.

L407: In this study, GCPs were not used, however,

Additional references

Hugelius, G., Loisel, J., Chadburn, S., Jackson, R. B., Jones, M., MacDonald, G., Marushchak, M., Olefeldt, D., Packalen, M., Siewert, M. B., Treat, C., Turetsky, M., Voigt, C., & Yu, Z. (2020). Large stocks of peatland carbon and nitrogen are vulnerable to permafrost thaw. Proceedings of the National Academy of Sciences, 117(34), 20438–20446. https://doi.org/10.1073/pnas.1916387117

Putkonen, J., & Roe, G. (2003). Rain-on-snow events impact soil temperatures and affect ungulate survival. Geophysical Research Letters - GEOPHYS RES LETT, 30, 37–1. https://doi.org/10.1029/2002GL016326

Sjöberg, Y., Coon, E., K. Sannel, A. B., Pannetier, R., Harp, D., Frampton, A., Painter, S. L., & Lyon, S. W. (2016). Thermal effects of groundwater flow through subarctic fens: A case study based on field observations and numerical modeling. Water Resources Research, 52(3), 1591–1606. https://doi.org/10.1002/2015WR017571

Taylor, J. R. (1997). Introduction to Error Analysis, the Study of Uncertainties in Physical Measurements (2nd ed.). University Science Books, ISBN 093570275X

Valman, S., Siewert, M. B., Boyd, D., Ledger, M., Gee, D., de la Barreda-Bautista, B., Sowter, A., & Sjögersten, S. (2024). InSAR-measured permafrost degradation of palsa peatlands in northern Sweden. The Cryosphere, 18(4), 1773–1790. https://doi.org/10.5194/tc-18-1773-2024

Walvoord, M. A., & Kurylyk, B. L. (2016). Hydraulic impacts of permafrost thawing and implications for groundwater fluxes in the Arctic. Water Resources Research, 52(2), 1236–1255. https://doi.org/10.1002/2015WR018299

Zhang, T. (2005). Influence of the seasonal snow cover on the ground thermal regime: An overview. Reviews of Geophysics - REV GEOPHYS, 43. https://doi.org/10.1029/2004RG000157

Dear Editor,

Thank you for considering our manuscript egusphere-2024-141 ("Multitemporal UAV LiDAR detects seasonal heave and subsidence on palsas") for publication in The Cryosphere. We have been through all feedback provided by you and the reviewers, and we are glad to report that all comments led to changes in the manuscript one way or the other.

In the below, we provide a point-to-point reply to each comment/question raised in RC2, and we specify the changes that were implemented in the manuscript for each of them.

Q = Question / comment raised

A = Answer / details of the changes made

LXXX–XXX refers to the line numbers of text in the revised manuscript.

General comments:

Q1: The paper is well written. However, I think the opening paragraph in particular is the weakest part of the writing because it is trying to address too many points with too little detail. I recommend splitting this paragraph into two (e.g. 1: The ecological and climatic importance of permafrost, and 2: threats to permafrost environments).

A1: First of all, we thank the reviewer for stating that the paper is well written. They suggest splitting up the first paragraph of Chapter 1 as it tries to address to many points, without enough details. After their comment, we agree with that some of the points deserve more detail and that the paragraph can be split up in two. The main focus of our study are the seasonal palsa dynamics and the use of UAV LiDAR for monitoring permafrost environments. We therefore try to not create too long of an introduction regarding the general loss and threats to permafrost regions. While the 'ecological and climatic importance of permafrost' is inherently linked to the 'threats to permafrost environment', we have followed the suggestion and spit up the first paragraph.

In the first, we have now addressed the important role of peatlands in the permafrost zone related to their carbon stocks.

L25–33 In the face of accelerating climate change, permafrost – defined as ground that remains at or below 0 ∘C for at least two consecutive years (Harris et al., 1988) – is warming at a global scale (Biskaborn et al., 2019). Permafrost regions hold approximately 50% (1300±200 Pg) of the world's terrestrial carbon, making them vital to the global climate system (Hugelius et al., 2020). A significant amount (415±150 Pg carbon) is stored in northern peatlands, nearly half of which is affected by permafrost (Hugelius et al., 2020). In the discontinuous and sporadic permafrost zones, peatland permafrost can be found in palsa mires, consisting of peat plateaus and palsas. Palsas are peat mounds with a core of perennially frozen soil (Seppälä, 1986). Palsa mires are a sensitive and heterogeneous ecosystem, which are vulnerable to increased air temperatures and precipitation in the Arctic (Luoto et al., 2004).

The second paragraph now includes more examples of threats to palsa mires as permafrost environment.

L34–50 The climatic space for palsas, typically with a mean annual air temperature between -3 °C and -5 °C and mean annual precipitation <450 mm, according to Luoto et al. (2004a), is projected to disappear in Fennoscandia by the end of the 21st century (Fewster et al., 2022). In recent studies, an increasing lateral degradation rate of palsas is reported (Borge et al., 2017; Mamet et al., 2017; Olvmo et al., 2020) which may have far-reaching consequences for these ecosystems and biodiversity of the subarctic region (Luoto et al., 2004; Swindles et al., 2015). For example, the loss of palsas can lead to the decline of specialized plant species that are adapted to the unique, dry conditions of palsas. Additionally, animals that depend on these habitats, such as certain bird species and small mammals are affected (Luoto et al., 2004). In addition to the threat to biodiversity, the degradation of palsas also impacts reindeer herding, berry picking and

transport for local communities, as these elevated, often dry, parts of the landscape shrink and become more fragmented. The transition from a palsa to a lower lying, wet fen, is also associated with an increase in CH_4 and CO_2 emissions (e.g. Łakomiec et al., 2021; Pirk et al., 2024; Swindles et al., 2015; Voigt et al., 2019) as the stored carbon in these peatlands is subject to microbial re-mobilization when permafrost thaws. The climatic feedback mechanism further highlights the need for continued monitoring of these environments. Therefore, palsa mires are a priority habitat of the EU Species and Habitat Directive (EUNIS -Factsheet for Palsa Mires, 2013). However, in Sweden only about half (47%) of the total palsa area is situated within a protected area (Backe, 2014).

Q2: Given the limited spatial and temporal scope of the paper, some further work is needed to contextualise the findings at these sites with other literature from the region. I note that comparisons are already made with site-specific studies using LiDAR but in Alaska and Canada. Within Scandinavia, methodological comparisons are made with other studies (e.g. use of InSAR vs LiDAR) but the findings of these studies could also be incorporated to better understand trends at this site and the region. Whilst InSAR is broadly agreed to underestimate rates, there is confidence in the direction of vertical trends, which can still make for valuable contextual information. I recommend taking a look at the very recently published paper from Valman et al. (2024) [https://doi.org/10.5194/tc-18-1773-2024], which looks at the subsidence of the same site of Vissátvuopmi (and across the same palsa mire complex more broadly) except using InSAR from 2017-2021. It could provide a site history and context of subsidence trends prior to your study embarking in 2022 (may be useful at lines 258-267).

A2: The reviewer states that the paper can be improved by providing more context of other studies done in the region. We value this comment and have taken several approaches in order to contextualize our findings. First of all, we have provided more context of Vissátvuopmi as part of the eight named palsa complexes in Sweden using the findings of Valman et al. (2024):

L90–95 Located near the Finnish border, and just southwest of the Könkämäeno river, Vissátvuopmi is the largest, of the in total eight named, coherent palsa mire complexes in Sweden (ca. 150 ha of palsa area; Backe, 2014) at N 68°47'50", E 21°11'30" (Fig. 1). According to InSAR data from 2017, 55% of the total area of these eight palsa complexes is subsiding, compared to 98% of the Vissátvuopmi area (Valman et al., 2024). Though notably, only Vissátvuopmi and Árbuvuopmi (northwest of Vissátvuopmi) are not part of the EU Natura 2000 network.

Next, in order to further contextualize our results, we include the findings by de la Barreda-Bautista et al. (2022) and the recently published Valman et al. (2024), as the reviewer suggested. We have noticed this recent publication and agree that it provides as very suitable context of longer-term subsidence of palsa complexes in the region.

L339–351: de la Barreda-Bautista et al. (2022) reported a maximum subsidence rate of 1.5 cm, from InSAR data, between 2017 and 2020 on a palsa plateau at ca. 100 km from the Vissátvuopmi palsa complex. Due to the coarser spatial resolution (20 m) of the data, it is likely to

underestimate actual heave and subsidence values of smaller isolated features such as palsas. Over the same period and location, they observed 25 cm subsidence from DEMs created with UAV photogrammetry. InSAR subsidence has also been analyzed at the Vissátvuopmi palsa complex (Valman et al., 2024). They found that Vissátvuopmi and the adjacent Árbuvuopmi are the fastest subsiding complexes of the eight studied in northern Sweden, with maximum subsidence rates of -8.9 and -9.9 mm yr-1 between 2017 and 2021. While the absolute values are not comparable with subsidence rates from our UAV LiDAR data due to the large discrepancy in spatial resolution, they give an important context of the subsidence trend across the entire palsa complex in the years right before our study period. The fact that Vissátvuopmi is among the most quickly deforming complexes and at the same time does not hold a protected status, emphasizes the importance of studies conducted here.

Finally, we have incorporated a more in-depth comparison with the findings from Olvmo et al. (2020), who provide annual (lateral) decay rates, at the same palsas that we studied, based on historical orthophotos. We have used orthophotos that were created with UAV photographs at the same day as the LiDAR surveys to delineate the palsas and find the area of the palsas in September 2023. We were then able to compare annual decay rates from 2010–2016 and 2016–2023 on the Dome and Ridge palsa.

L387–394: Olvmo et al. (2020) found an average annual decay rate (loss of palsa area) of -0.74 %a−1 and -2.45 %a−1 for the Dome and Ridge palsas respectively, for the period 2010–2016. Using the palsa area from Olvmo et al. (2020) in 2016 and the extent in 2023 from our study, we can calculate a new annual decay rate. For the period 2016–2023, we found respective rates of -3.27 %a−1 and -1.55 %a−1. The -2.53 %a−1 change in decay rate on the Dome palsa can be largely explained by the degradation hotspot, which covered ca. 2.6% of the total palsa area. The slight decrease in annual decay rate on the Ridge palsa could be explained by a stabilization of degraded areas. When excluding the degradation hotspot on the Dome palsa, the Ridge palsa lost a larger percentage of its extent, similar to Olvmo et al. (2020).

Specific comments:

Q3: L21: replace "helps in" with "facilitates"

A3: We agree with the suggestion and made the adjustment

L21–22: It facilitates tracking the ongoing effects of climate change and highlights palsa dynamics that would not be captured by annual measurements alone.

Q4: L45: it would be useful to include a definition of 'lateral erosion' and 'vertical subsidence' and differentiate between the two here.

A4: We agree with the reviewer that a more elaborate definition of 'lateral erosion' and 'vertical subsidence' will improve this part of the Introduction chapter. The revised text is as follows:

L51–55: The degradation of permafrost in palsas is indicated by both lateral erosion and vertical subsidence. Lateral erosion refers to the horizontal shrinkage of the permafrost body along the edges of palsas, often resulting in the formation or expansion of connected water bodies, i.e. thermokarst lakes (Martin et al., 2021). Vertical subsidence, on the other hand, involves the downward sinking of the ground surface as a result of the melting of excess ground ice, leading to a drop in surface elevation.

Q5: L79-81: I would reserve stating findings until the discussion/conclusion.

A5: After revising the Introduction, we agree that this belongs in the Conclusions and have removed this sentence.

Q6: L92: I am not familiar with what an ATV is. Please define.

A6: We have now included the definition of ATV, all-terrain vehicle.

L105–106 An all-terrain vehicle (ATV) track runs over the northeastern part of the palsa,

Q7: L116: Please define HOBO weather station.

A7: HOBO is a datalogger brand by Onset Computer Corporation. Their weather stations are widely used for environmental monitoring. In order to clarify this, we have changed the text.

L130–132: In September 2022, a HOBO® U30-NRC (Onset Computer Corporation) weather station was set up in the nearby settlement of Saarikoski, ca. 1.5 km from the study site (see Fig. 1b for location of the two weather stations).

Q8: L152: change 'm2' to 'm^2'

A8: We thank the reviewer for pointing out this mistake and have fixed it.

L171–172: Similarly, flights over the Dome palsa yielded a slightly larger coverage area of 53993 m^2 compared to the Ridge palsa,

Q9: L206: "palsas palsa" repeated twice in caption

A9: Thank you again for finding this language mistake. We also took the opportunity to fix the incorrect naming of fig. 5c and d from 'DTM' to 'difference map'. We have adjusted the caption.

L238–242: Figure 5. DTMs of the Dome (a,b) and Ridge (d,e) palsas on UAV LiDAR scans in September 2022 and September 2023. The black lines represent the extent of the palsas, based on orthomosaics from the same day as the UAV LiDAR surveys. The difference maps (c,f) show the topographical changes over one year, with the palsa extent from the September 2022 flights in black The dashed box in (c) shows the 'degradation hotspot' on the Dome palsa.

Q10: L212: two full stops here – please remove one.

A10: We have removed the second stop.

L270–272: The snow thickness is up to ca. 2.0 m at the eastern margin of both palsas and 1.0 to 1.5 m in the depressions, while the crests remain snow-free (also see Fig. 1d).

Q11: L228: could you clarify what you mean by "deepening" here? I presume this is referring to snow depth?

A11: The 'deepening' here refers to the subsidence that occurred in the all-terrain vehicle (ATV) track. This was the only part in the text that the term 'deepening' was used and we replaced it by 'subsidence' in order to be consistent.

  The ATV track that crosses the Dome palsa shows a subsidence of 0.2–0.3 m just over the time period in this study (at ca. 27–29 m in Fig. 7e).

Q12: L276-277: Glad to see that you have taken this into account – I would be intrigued to find out more about how you corrected for this effect? Elevational changes in the mire could be partially independent of the palsa elevational changes because 'mire breathing' may reflect water table level change (if water table rises above ground level) rather than ground surface level change at some points during the seasonal cycle. I am not sure if this is the case at the sites you have investigated. In any case, some site context may be useful here to establish whether water tables typically rise above mire surface level here and how you would have corrected for this. If so, it's possible this could have further implications for lateral erosion rates? You may prefer to address this in the methods.

A12: We thank the reviewer for pointing out that the Method section was missing details on this part. These two palsas are close to a mountain and surrounded by mostly dry, walkable terrain and water tables typically do not rise above the mire surface in most of the surroundings of the two studied palsas, except for thermokarst lakes (or ponds) that border the palsa. To clarify this, we have first made adjustments in the Study site chapter:

L99–101: Water tables typically do not rise above the mire surface in most of the surroundings of the two studied palsas, except for thermokarst ponds that border the palsas

Additionally, we made the orthophoto of the site (Fig. 1c) clearer, by moving the site photos (Figs. 1d and 1e):
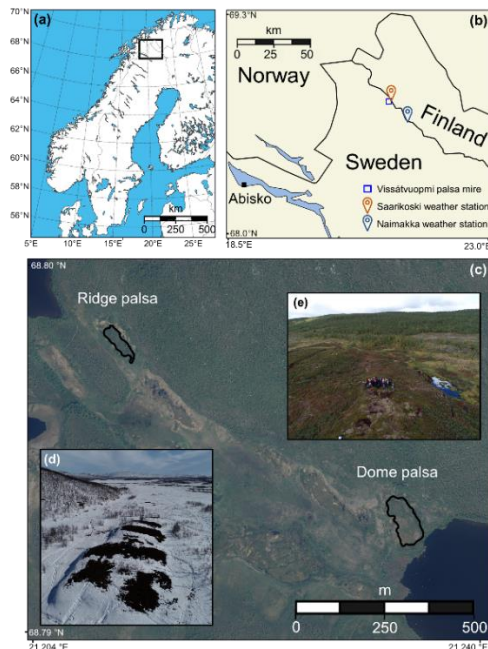
The polygons around the palsas that we used to transform the elevation to height are carefully drawn on the areas that were dry at the moment of all the flights and thus no open water is included. That means that changes in the water table, where above the ground surface, are not interfering with the normalization calculation. An important note to make is that the definition of a palsa is morphological and thus per definition the height above the surroundings is the height of the palsa.

The Methods chapter is now changed as follows:

L218–226 For each DTM, the mean elevation of the palsa's surrounding was computed and subtracted from the DTM, which normalizes the elevation of the palsa into the height above the surroundings. Since the definition of palsas is morphological (Harris et al., 1988), the height above its surroundings is per definition the height of the palsa. For the normalization, we used the previously mentioned orthophotos to create a polygon around each palsa, for which the mean elevation was taken per LiDAR flight. Areas containing open water at any of the time steps, either thermokarst lakes directly around the palsas or other ponds, were not included in these polygons. The transformation from elevation to height, simplifies the comparison between the data from the different flights.

The final point made by the reviewer regards whether the water that surrounds the palsas has further implications for lateral erosion rates. There is indeed consensus that this is the case. E.g. Martin et al. (2021) and Sjöberg et al. (2016) describe the importance of lateral water and associated heat fluxes for permafrost degradation. From our frequent field visits, we know that the Ridge palsa is surrounded by relatively larger and deeper thermokarst ponds compared to the Dome palsa, which affects water and heat fluxes into the palsa. By comparing the lateral extent from our study to that in in Olvmo et al. (2020), we find a higher annual decay rate in the Dome palsa between 2016 and 2023 (while they found the opposite for the period 2010–2016). However, this difference can be entirely explained by the degradation hotspot on the Dome palsa, for which the initiation is not fully known. To find a more direct effect of the water bodies on the lateral erosion rates, we need to conduct geophysical investigations of the interior of the palsas and their surroundings.

These points are now also discussed in the main text, also as part of Q2 in this response, where we aim to contextualize our findings with data from previous studies in the region.

L387–398: Olvmo et al. (2020) found an average annual decay rate (loss of palsa area) of -0.74 %a−1 and -2.45 %a−1 for the Dome and Ridge palsas respectively, for the period 2010–2016. Using the palsa area from Olvmo et al. (2020) in 2016 and the extent in 2023 from our study, we can calculate a new annual decay rate. For the period 2016–2023, we found respective rates of -3.27 %a−1 and -1.55 %a−1. The -2.53 %a−1 change in decay rate on the Dome palsa can be largely explained by the degradation hotspot, which covered ca. 2.6% of the total palsa area. The slight decrease in annual decay rate on the Ridge palsa could be explained by a stabilization of degraded areas. When excluding the degradation hotspot on the Dome palsa, the Ridge palsa lost a larger percentage of its extent, similar to Olvmo et al. (2020). Again, lateral water

fluxes greatly affect ground temperatures and permafrost degradation (Martin et al., 2021; Sjöberg et al., 2016; Walvoord & Kurylyk, 2016). Therefore, smaller palsas are relatively more susceptible to lateral erosion through heat and water fluxes, provided by surrounding thermokarst ponds, compared to larger palsas (e.g. Borge et al., 2017).

L355–359: The Ridge palsa is surrounded by relatively larger and deeper thermokarst ponds, which could enhance vertical subsidence more centrally in the palsas as a result of increased heat transfer to the palsa core. To find out if the higher subsidence on this palsa is a robust signal and what processes are responsible for this, continued annual LiDAR surveys and observations of the palsa's interior via geophysical imaging are needed.

Q13: L279: replace "been" with "used".

A13: We agree with the language suggestion and have changed the sentence accordingly.

L328–329: While other studies have applied multitemporal LiDAR for detecting permafrost dynamics, they have used terrestrial LiDAR scanning

Q14: L289-307: you could also consider higher winter precipitation rates contributing to greater thaw over the following summer season, especially with warmer winter temperatures so that rain falls instead of snow. This could compromise snow depth over the winter and therefore increase the length of the following thaw period. It's possible that this can be seen from the weather station data in Figure 2, where it looks like there is lower average snow depth and greater winter precipitation rates in the winter season 2022/2023.

A14: We appreciate the effort of the reviewer to explain the findings of our study, especially regarding the 'degradation hotspot' in the nw part of the Dome palsa. The suggestion of higher winter precipitation rates (and a longer thawing season) playing a part in initiating this degradation, is valuable. We therefore included the following text:

L373–377: Additionally, the precipitation in this winter was greater than the previous winter, which may have caused additional warming of the ground, either via a thicker snowpack (T. Zhang, 2005) or latent heat brought by rainfall (Putkonen & Roe, 2003). This falls in line with Olvmo et al. (2020), who conclude that increased winter precipitation is one of the main causes of rapid palsa degradation in the study region.

It is important to note that the snow depth is recorded at ca. 1.5 km from the palsas, where local topography affects the snow distribution in a different way than directly on the palsa surface. Hence the slightly differing snow depth between the different winters may not reflect the snow depth on the palsas. Also, a thicker snowpack is generally related to increased ground temperatures and active layer thickness due to the insulating effect of snow. The increased

precipitation (both as rain and snow), as suggested by the reviewer, could thus contribute to a warmer soil.

Q15: L319: two commas, remove one.

A15: We have removed the second comma.

L407: In this study, GCPs were not used, however,

Q16: L366: insert "of" between "degradation palsas"

A16: We thank the reviewer for this final language suggestion and have adjust the text.

L458–460: This substantial permafrost degradation occurred between September 2022 and April 2023 which suggests that the degradation of palsas is not limited to the summer months.

Additional references

Hugelius, G., Loisel, J., Chadburn, S., Jackson, R. B., Jones, M., MacDonald, G., Marushchak, M.,
Olefeldt, D., Packalen, M., Siewert, M. B., Treat, C., Turetsky, M., Voigt, C., & Yu, Z. (2020).
Large stocks of peatland carbon and nitrogen are vulnerable to permafrost thaw. Proceedings of
the National Academy of Sciences, 117(34), 20438–20446.
https://doi.org/10.1073/pnas.1916387117

Putkonen, J., & Roe, G. (2003). Rain-on-snow events impact soil temperatures and affect ungulate
survival. Geophysical Research Letters - GEOPHYS RES LETT, 30, 37–1.
https://doi.org/10.1029/2002GL016326

Sjöberg, Y., Coon, E., K. Sannel, A. B., Pannetier, R., Harp, D., Frampton, A., Painter, S. L., & Lyon, S.
W. (2016). Thermal effects of groundwater flow through subarctic fens: A case study based on
field observations and numerical modeling. Water Resources Research, 52(3), 1591–1606.
https://doi.org/10.1002/2015WR017571

Taylor, J. R. (1997). Introduction to Error Analysis, the Study of Uncertainties in Physical Measurements
(2nd ed.). University Science Books, ISBN 093570275X

Valman, S., Siewert, M. B., Boyd, D., Ledger, M., Gee, D., de la Barreda-Bautista, B., Sowter, A., &
Sjögersten, S. (2024). InSAR-measured permafrost degradation of palsa peatlands in northern
Sweden. The Cryosphere, 18(4), 1773–1790. https://doi.org/10.5194/tc-18-1773-2024

Walvoord, M. A., & Kurylyk, B. L. (2016). Hydraulic impacts of permafrost thawing and implications for
groundwater fluxes in the Arctic. Water Resources Research, 52(2), 1236–1255.
https://doi.org/10.1002/2015WR018299

Zhang, T. (2005). Influence of the seasonal snow cover on the ground thermal regime: An overview.
Reviews of Geophysics - REV GEOPHYS, 43. https://doi.org/10.1029/2004RG000157